A Database of Phase Calibration Sources for the Giant Metrewave Radio Telescope

Dharam Vir LAL, Shilpa S. DUBAL & Sachin S. SHERKAR

September 15, 2016

Contents

List of Figures

List of Tables

Overview

We are pursuing a project to build a database of phase calibration sources suitable for Giant Metrewave Radio Telescope (GMRT). In this report we present the first release of 45 low frequency calibration sources at 235 MHz and 610 MHz. We provide their flux densities, models for calibration sources, (u, v) plots, final deconvolved restored maps and CLEAN-component lists/files for use in the Astronomical Image Processing System (AIPS) and the Common Astronomy Software Applications (CASA). We also assign a quality factor to each of the calibration sources. These data products are made available online through the GMRT observatory website (available at `http://gmrt.ncra.tifr.res.in`).

1 Introduction

The GMRT (Swarup et al.1991) is the most sensitive radio telescope in the world that is capable of operating at low radio frequencies from 150 MHz to 1450 MHz. In order to obtain reliable information about target astronomical sources, radio sources whose structure and flux density are known *a priori* are routinely observed to determine antenna based calibration solutions. Any errors in the models used for these calibration sources reflect in errors in the antenna based calibration solutions, especially in the phase, and limit the quality of the radio images obtained. GMRT users have traditionally been using phase calibration sources from the Very Large Array (VLA) calibrator manual, which is biased towards observations optimized for higher frequencies.

In this report, our motivations for such a database are discussed in Sect. 2. The sample is presented in Sect. 3 and its archival data and data reduction are detailed in Sect. 4 and Sect. 4.1, respectively. The results from the database, i.e., their quality standards and sky distribution are discussed in Sect. 5.1 and Sect. 5.2, respectively, and a summary in Sect. 6.

2 Motivations

The process of removing effects of phase and amplitude corruption from interferometer data is called calibration (Fomalont & Perley 1999). Several complexities and levels in the calibration of interferometric instruments exist, for example, errors due to (i) changes in the length of transmission system or receiver sensitivity and the electronics, (ii) inaccurate antenna positions (i.e., geometric errors), which are typically known to $\approx$ cm–m, and (iii) changes in the visibility induced by the atmosphere, including ionosphere (Beasley & Conway 1995). The observed visibility phase is defined as the relative phase of the electric fields measured simultaneously at two points along the wavefront from the radio sources. The atmospheric effects on this phase can be important on timescales ranging from less than a minute to hours or more.

Mathematically, the error in observed visibility phase $\phi_{\rm obs}(t,\ \nu)$ from the correlator can be expressed as

$$\phi_{\rm obs}(t,\ \nu) = \phi_{\rm true}(t,\ \nu) + \phi_{\rm inst}(t,\ \nu) + \phi_{\rm geom}(t,\ \nu) + \phi_{\rm atmos}(t,\ \nu)$$

where $\phi_{\rm true}(t,\ \nu)$ is the true visibility phase, $\phi_{\rm inst}(t,\ \nu)$ is the sum of all instrumental phase errors at the two antennas and is possibly due to propagation through the antenna optics and electronics before the sampled electric field is digitized, $\phi_{\rm geom}(t,\ \nu)$ is the phase error due to geometrical errors in the delay model and $\phi_{\rm atmos}(t,\ \nu)$ represent the effects of different atmospheric delays above each antenna. Note that both the ionospheric and the tropospheric (Thompson et al. 2001) errors are included in phase errors due to the atmosphere. The dominant sources of errors at low frequencies ($\lesssim$ 1 GHz) are refraction, propagation delay and Faraday rotation caused by the ionosphere, while at high frequencies ($\gtrsim$ 1 GHz) they are scattering, effects of water vapor and propagation delay caused by the troposphere (Thompson et al. 2001). Instrumental, $\phi_{\rm inst}(t,\ \nu)$ and geometrical, $\phi_{\rm geom}(t,\ \nu)$ errors can be reduced to acceptable levels by good design, but corrections for changes in the visibility due to the atmosphere are not possible, since these changes affect visibility phases. It is well known that the ionosphere severely limits the phase stability of radio interferometers at low radio frequencies (Intema et al. 2009). In practice, if $\phi_{\rm obs}(t,\ \nu)$ varies by a full turn over time or frequency-channel, it limits an observer's ability to integrate data over time and frequency.

The technique of making observations of a bright nearby point source, called the 'phase' calibration source, frequently interspersed with the target source is called phase referencing (Beasley & Conway 1995). This technique of phase referencing has been used successfully to allow correction of the fast temporal changes of relative phases of individual antennas of the interferometer.

Table 1: The observing log for phase calibration sources.

			235 MHz			610 MHz		
Calibrator (J2000)	Obs-date	Flux density calibrator	$\Delta\nu$ (MHz)	t_{int} (min)	Synthesized, P.A. beam (arcsec^2, deg)	$\Delta\nu$ (MHz)	t_{int} (min)	Synthesized, P.A. beam (arcsec^2, deg)
(1)	(2)	(3)	(4)	(5)	(6)	(7)	(8)	(9)
0010−418	2013-07-05	3C48	16 / 15.2	67	21.5 × 10.3, 21.6	32 / 31.2	85	14.3 × 6.5, 14.8
0029+349	2006-07-10	3C48	16 / 14.9	33	13.2 × 9.9, 41.9	32 / 30.8	33	5.4 × 4.1, 50.3
0119+321	2007-08-17	3C48	6 / 5.4	58	14.1 × 9.7, 71.7	32 / 30.8	58	6.0 × 4.7, 82.5
0410+769	2005-01-22	3C147	6 / 4.9	167	18.0 × 14.6, −86.3	16 / 15.0	173	10.8 × 5.8, −68.8
0745+101	2011-11-17	3C48				16 / 15.2	89	7.1 × 6.1, 37.2
0943−083	2008-12-05	3C48				16 / 15.2	71	5.3 × 4.8, 27.8
1130−148	2009-06-06	3C286	6 / 5.2	53	16.3 × 10.8, 21.3	32 / 31.4	53	7.1 × 4.6, 21.2
1313+675	2011-02-12	3C147	6 / 4.9	48	16.9 × 13.1, −53.2	32 / 31.0	48	6.5 × 5.4, −51.8
1400+621	2004-01-02	3C48				16 / 14.6	62	9.3 × 5.0, −45.6
1445+099	2008-07-22	3C147	6 / 5.1	52	12.0 × 10.1, 84.1	32 / 31.2	62	5.2 × 4.2, 59.6
1602+334	2009-06-06	3C286	6 / 5.1	51	12.6 × 10.1, 5.8	32 / 31.4	51	5.7 × 5.0, 9.4
1944+548	2013-07-12	3C48	16 / 15.3	57	14.8 × 11.8, −50.8	32 / 31.0	57	6.1 × 5.1, −49.0
2011−067	2008-12-06	3C286	6 / 4.9	25	14.6 × 9.6, 48.0	32 / 31.2	65	5.6 × 4.6, 48.1
2212+018	2008-08-10	3C147	6 / 5.3	34	14.8 × 11.0, 32.0	32 / 31.2	34	6.2 × 5.3, −1.3
2344+824	2013-07-24	3C48	16 / 15.1	49	23.5 × 9.4, −54.1	32 / 31.0	49	12.2 × 5.3, −62.4
2355+498	2013-07-24	3C48	16 / 15.1	24	15.0 × 9.5, −52.1	32 / 31.0	50	8.5 × 4.7, −74.1
0024−420	2013-07-05	3C48	16 / 15.2	67	21.5 × 10.3, 21.6	32 / 31.2	84	10.8 × 6.6, 18.8
0059+001	2006-07-22	3C48	6 / 5.2	36	13.4 × 10.3, 57.3	32 / 31.3	67	6.3 × 4.7, 62.7
0102+584	2013-07-12	3C48	16 / 15.3	55	12.1 × 9.6, −6.9	32 / 31.3	57	5.9 × 4.6, 6.6
0136+478	2013-07-12	3C48	16 / 15.3	37	12.0 × 9.7, 29.2	32 / 31.0	57	5.3 × 4.2, 27.2
0217+738	2013-07-12	3C48	16 / 15.3	10	18.6 × 9.0, 1.8	32 / 31.0	58	7.7 × 4.5, 11.9
0238+166	2007-08-17	3C48	6 / 5.4	45	14.8 × 11.3, −89.5	32 / 30.8	45	7.4 × 4.7, 85.6
0240−231	2008-07-21	3C147	6 / 5.1	63	15.6 × 12.1, −17.7	32 / 31.2	63	6.9 × 5.2, −13.0
0303+472	2009-10-25	3C48	6 / 5.0	99	13.5 × 10.8, 66.9	32 / 31.4	99	6.2 × 5.3, −77.4
0414+343	2013-07-26	3C48	16 / 15.1	57	11.2 × 7.9, 54.3	32 / 31.0	57	5.5 × 4.5, 73.1
0555+398	2009-11-20	3C147				16 / 15.2	57	6.3 × 4.2, 75.2
0607−085	2008-08-10	3C147	6 / 5.3	25	15.2 × 11.2, 14.1	32 / 31.2	22	7.0 × 5.1, −8.0
0739+016	2008-07-21	3C147	6 / 5.1	61	13.8 × 11.4, −75.4	32 / 31.2	61	6.3 × 4.8, −60.0
1150−003	2008-07-22	3C48	6 / 5.1	67	13.2 × 12.2, 71.1	32 / 31.2	67	5.7 × 4.7, 59.1
1254+116	2008-07-21	3C147	6 / 5.1	54	13.0 × 10.5, 63.1	32 / 31.2	54	5.1 × 3.6, 63.9
1613+342	2002-12-21	3C286	6 / 4.9	48	17.4 × 10.6, −79.7	6 / 5.4	48	5.2 × 4.9, 68.9
1743−038	2006-07-20	3C286	6 / 5.2	55	13.8 × 11.8, 56.6	32 / 31.3	54	6.8 × 4.9, 28.6
1923−210	2008-07-22	3C147	6 / 5.1	53	14.6 × 10.8, 23.3	32 / 31.2	53	6.4 × 4.3, 26.7
2005+778	2013-07-12	3C48	16 / 15.3	56	22.1 × 11.9, −37.7	32 / 31.0	57	8.6 × 4.6, −34.3
2015+371	2013-08-13	3C48	16 / 15.0	57	19.7 × 12.3, 84.1	32 / 31.0	57	8.1 × 5.0, 82.3
2025+337	2013-08-13	3C48	16 / 15.0	55	20.8 × 12.8, 79.2	32 / 31.0	55	8.5 × 5.0, 77.8
2202+422	2013-08-02	3C48	16 / 15.0	48	11.3 × 10.7, 65.2	32 / 31.0	48	7.0 × 4.9, −69.3
2236+284	2008-08-10	3C147	6 / 5.3	21	14.7 × 12.2, −44.7	32 / 31.2	21	6.9 × 5.0, −48.2
2254+247	2013-07-24	3C48	16 / 15.1	44	16.4 × 10.2, 75.5	32 / 31.0	44	9.9 × 4.7, 87.2
0110+565	2003-01-13	3C147	6 / 5.3	69	14.8 × 11.0, 45.0	6 / 5.4	69	6.1 × 4.9, 54.5
0321+123	2004-03-27	3C286				16 / 15.2	91	7.3 × 5.0, 17.4
0438+488	2013-07-26	3C48	16 / 15.1	46	13.0 × 8.7, 53.5	32 / 31.0	57	6.0 × 4.6, 56.7
0632+103	2004-07-24	3C147	6 / 4.9	63	13.0 × 10.4, 71.6	32 / 31.0	64	7.7 × 4.1, 57.8
1513+236	2008-07-27	3C286	6 / 5.1	44	13.2 × 10.8, 72.0	32 / 31.2	49	5.6 × 4.5, 66.9
2023+544	2013-07-12	3C48	16 / 15.3	32	13.7 × 11.1, −23.4	32 / 31.0	56	6.0 × 5.3, −34.9

3 Sample

The VLA varies its angular resolution through movement of its antennas, and hence has four basic antenna configurations, A, B, C and D, whose scales vary by the ratios 35.5:10.8:3.28:1 (VLA observational status summary). GMRT, unlike the VLA, has a hybrid configuration, with 14 antennas in a central array and the remaining 16 antennas spread across three arms of a 'Y' (Swarup et al. 1991). The quality of VLA calibration sources varies with frequency and configuration (VLA observational status summary). Their absolute position errors range from $<$0.002 arcsec (code 'A', VLA observational status summary) to $>$0.15 arcsec (code 'T', VLA observational status summary). Correspondingly the phase calibration errors have several levels, from as small as $<$3% errors (P-class) or 10% errors (S-class) to confused or to unknown or inappropriate. We selected a list of target calibration sources from the VLA calibrator manual which met the following criteria: The source should be bright, i.e., have flux density at 20 cm, $S_{20\ \rm cm} > 0.5$ Jy and (i) should be P-class at A-array and B-array VLA configurations, and (ii) either P-class or S-class at C-array and D-array VLA configurations. These criteria provided us with 121 sources, whose positional uncertainties in right ascension and declination are $<$ 0.15 arcsec (VLA observational status summary). We used this list of 121 phase calibration sources to look for archival GMRT data and found observations for 45 (34%) sources listed in Table 1 at 235 MHz and 610 MHz. New observations were made only for a handful of sources when the archival data were badly affected by radio frequency interference (RFI) or challenging ionospheric conditions; otherwise no new GMRT observations were made for this project.

4 Archival Data

Typical GMRT continuum observations are bracketed and interleaved by primary (flux density and bandpass) calibration source scans on 3C 48, 3C 147 and 3C 286 of 10–20 minute duration. Interleaved in these observations are several secondary (phase) calibration source scans, each of a few minutes long duration. We extracted primary source and secondary calibration source scans from all the archival GMRT 235 MHz, 610 MHz data and dual frequency, both 235 MHz and 610 MHz data. Table 1 gives the details of the observations. The columns are as follows: (1) calibration source name. which encodes the J2000 position; (2) observing date; and (3) flux density and bandpass calibrator. Columns (4), (5) and (6), and (7), (8) and (9), respectively are for 235 MHz and 610 MHz data, where these columns are as follows: (4, 7) nominal and effective bandwidth; (5, 8) integration time; and (6, 9) FWHM of the elliptical Gaussian restoring beam and position angle (P.A.). These observations are usually performed in spectral line mode with the total number of channels ranging from 64 to 256 and from 128 to 512 at 235 MHz and 610 MHz, respectively, and widths of each channel ranging from 32.5 kHz to 125 kHz. Observations at 235 MHz for five sources, namely 0321+123, 0555+398, 0745+101, 0943−083 and 1400+621 were always affected severely by RFI or bad antennas.

4.1 Data Reduction

The raw telescope format data were converted to FITS and then analysed in AIPS using standard procedures. The flux density calibrators were used as an amplitude calibrator and to correct the bandpass shape. We used an extension of the Baars et al. (1977) scale to low frequencies and the uncertainty, both due to calibration and systematic typically is $\lesssim$ 5% (Lal & Rao 2007). The data were carefully inspected for bad antennas, scintillations and intermittent RFI, which were all flagged. Occasionally, we also used flagging and calibration (FLAGCAL) software pipeline (Prasad & Chengalur 2012, Chengalur 2013, Lal 2014) for automatic flagging and calibration of data. Typically $\lesssim$20% data were flagged for each calibration source. We left 3-5 channels on either side of the bandpass and the central channels of this flagged and calibrated data were averaged using the task SPLAT to reduce data volume.

The averaged data were subsequently used to make continuum images using the AIPS task IMAGR. While imaging, a mosaic of 55 and 37 slightly overlapping facets covering fields-of-view of $\sim$3.2 deg^2 and $\sim$0.5 deg^2 were used at 235 MHz and 610 MHz, respectively. Throughout the analysis, we ran IMAGR in 3–D mode for *w*–term correction and used 'uniform' weighting. The presence of a large number of sources in the field-of-view in each mapped field allowed us to perform 2–3 rounds of phase-only self-calibration, which was sufficient for the self-calibration process to converge. At each round of self-calibration, the image and the visibilities were compared to check for the improvement of the source model. The final mosaic of facet-images were stitched using task FLATN to construct a final model-image and corrected for the primary beam of the GMRT antennas. Table 2 lists flux densities of calibration sources at 235 MHz and 610 MHz, our GMRT measurements and rest of the measurements are gleaned from the VLA calibrator manual, and Fig. 1 presents their radio spectra.

Table 2: The integrated flux density (in Jy) and the quality factor for all 45 phase calibration sources.

Calibrator (J2000)	Frequency								Quality	
	235 (MHz)	610 (MHz)	1.42 (GHz)	5.00 (GHz)	8.10 (GHz)	15.00 (GHz)	23.06 (GHz)	42.83 (GHz)	235 (MHz)	610 (MHz)
0010−418	3.57	6.68	4.10	1.25	0.58	0.25			M	G
0024−420	4.01	3.23	2.80	1.70	0.94	0.40			M	M
0029+349	1.02	1.93	1.89	1.85	0.96	0.60	0.58	0.36	M	M
0059+001	4.70	3.61	2.50	1.35	0.96	0.70		0.42	M	G
0102+584	0.88	1.52	0.94	1.20	2.70	2.30		2.40	M	M
0110+565	3.93	2.78	1.90	0.85	0.53	0.30		0.11	M	M
0119+321	4.15	3.77	2.60	1.48	1.08	0.70		0.34	M	G
0136+478	1.09	1.24	1.62	1.88	1.80	1.60		1.60	M	M
0217+738	0.93	1.96	2.27	2.30	2.18	2.10		1.50	M	M
0238+166	0.96	1.49	1.26	1.73	1.30	3.30		3.50	M	M
0240−231	2.16	5.44	6.30	3.15	1.66	0.90	0.59	0.30	M	G
0303+472	1.74	0.94	1.80	2.47	1.43	2.90		1.20	M	M
0321+123		2.44	1.74	1.10	1.18	0.75				M
0410+769	9.65	8.15	5.76	2.79	2.21	1.46		0.66	M	G
0414+343	1.50	1.97	2.03	1.50	1.23	0.97		0.50	M	M
0438+488	3.95	2.36	1.37	0.54	0.34				M	G
0555+398		0.49	1.70	5.00	6.20	2.80		2.50		M
0607−085	3.57	3.02	3.00	2.70	3.22	2.10		3.60	M	M
0632+103	3.74	2.69	2.45	0.90	0.50	0.20		0.08	M	G
0739+016	1.50	1.64	1.95	1.80	2.00	2.05		2.10	M	M
0745+101		1.68	3.30	3.50	2.95	2.20				M
0943−083		3.01	2.70	1.20	0.68	0.40				M
1130−148	4.87	5.85	5.33	4.60	3.06	2.30		0.60	M	G
1150−003	3.20	3.64	2.80	1.92	1.25	1.40		0.65	G	G
1254+116	0.54	0.85	1.00	0.80	0.90	0.90		0.70	M	M
1313+675	6.39	4.38	2.40	0.90	0.60	0.30			M	G
1400+621		6.96	4.40	1.72	1.08	0.67	0.48	0.28		G
1445+099	0.97	2.39	2.60	1.20	0.73	0.40		0.10	M	G
1513+236	2.14	2.45	1.60	0.80	0.52			0.12	M	G
1602+334	2.21	3.03	2.60	2.00	2.05	1.40		0.41	M	G
1613+342	2.29	4.29	2.70	2.30	2.67	2.00		2.58	M	G
1743−038	1.11	1.29	1.55	2.70	3.80	3.80		5.10	M	M
1923−210	1.18	2.48	2.00		2.70			1.40	M	G
1944+548	0.77	1.96	1.66		0.67			0.15	M	M
2005+778	0.87	0.55	1.00	1.60	2.50	1.60		1.00	M	M
2011−067	0.45	2.24	2.60	1.30	0.85	0.49		0.80	M	G
2015+371	1.07	1.55	2.18	2.76	2.95	2.59		2.90	M	M
2023+544	0.92	1.33	1.20	1.05	1.00	1.10		0.70	M	M
2025+337	0.92	1.33	1.44	2.80	3.80	2.50	2.30	2.80	M	M
2202+422	2.69	4.78	6.07	5.40	3.95	3.50		2.50	M	G
2212+018	5.35	4.56	2.65	1.10	0.60			0.14	M	G
2236+284	0.75	0.83	1.50	2.00	0.90	1.50		0.80	M	M
2254+247	3.29	2.58	1.84	0.80	0.59	0.65		0.30	G	G
2344+824	5.69	5.46	3.79	1.34	0.75	0.40		0.30	M	G
2355+498	1.77	2.74	2.36	1.60	1.00	0.90		0.28	M	M

5 Results

5.1 Quality Factor

There are several criteria for choosing and including a calibration source, e.g., for correcting instrumental, geometric and atmospheric gains, both amplitude and phase variations, monitoring the quality of the data and for searching for occasional amplitude and phase jumps, if any. Unlike the quality standards, e.g., 'P', 'S', etc. of phase calibration sources from the VLA calibrator manual for the desired observing frequency and array configuration, which depend on morphology of each calibration sources and hence $(u,v)_{\rm min}$ and $(u,v)_{\rm max}$, it is difficult to provide similar quality classifications for GMRT calibration sources. This is because GMRT has a hybrid configuration (see also Sect. 3) whereby it samples the (u,v) plane adequately on the short baselines as well as on the long baselines, and its data often suffers from broadband RFI, and hence quantifying in absolute units of closure errors and therefore ascribing $(u,v)_{\rm min}$ and $(u,v)_{\rm max}$ limits to a calibration source is inefficient. Additionally, all models of calibration sources are self-calibrated, which provide us with adequate image models.

Here, instead we provide two qualities, good, 'G' or moderate, 'M' based on strength of the calibration source and strengths of all other sources detected in the field-of-view of the calibration source, which are above five times the root-mean-square noise. We henceforth describe all other sources detected in the calibration source field as the contaminants. Quantitatively, if a phase calibration source at the phase-centre has flux density $\gtrsim 1$ Jy and the contaminants in its field-of-view contribute up to $\lesssim$0.01 Jy is called a 'good' quality calibration source. The rest of the sources are qualified as 'moderate' in this criteria at both frequencies. Table 2 lists good, G or moderate, M for each of the 45 low frequency calibration sources at 235 MHz and 610 MHz. To compare this criterion of good or moderate with respect to criteria of the VLA calibrator manual, the contribution to the expected closure errors due to unmodeled phase of the contaminants corresponds to 10% or less for good, and more than 10% for moderate calibration sources. Note that since, we are providing a model for each calibration source field, the closure error is much less, $\lesssim$3%, irrespective of whether the calibration source is a good, G or a moderate, M.

5.2 Sky Distribution

The distribution of these phase calibration radio sources on the sky reflects the structure of the observable universe on the largest possible scales that can be mapped with the GMRT via the phase-referencing technique. Fig. 2 shows the distribution of phase calibration sources on the celestial sphere. The smallest and the largest angular separations between any two phase calibration sources are $\sim$0.5 deg and $\sim$52 deg, respectively. Thus, it is possible that for a certain observation the target source may be as far as $\sim$26 deg from the nearest phase calibration source, more than the recommended proximity between the calibration source and the target source (VLA observational status summary); clearly, our ongoing efforts to increase the size of the database would address this concern.

6 Summary

The data products are available through the GMRT observatory website (`http://gmrt.ncra.tifr.res.in`) and is a valuable database in planning a GMRT observation, be it spectral-line or continuum or pulsar. We provide flux densities, models, (u,v) plots, final deconvolved restored maps and CLEAN-component lists/files covering fields-of-view of $\sim$4 deg^2 and $\sim$0.5 deg^2 at 235 MHz and 610 MHz, respectively, for use in the AIPS and the CASA for each calibration source. We also assign a quality factor for each of the calibration sources. The distribution of these 45 phase calibration sources in the sky is uniform with no visible large gaps or voids in the sky. Our ongoing efforts to increase the size of this database would often provide a suitable choice of a phase calibration source that is within 20 deg to a given target source. A screen-shot of the GMRT calibrator manual from the online web-page is shown in Fig. 3. The database at these two frequencies also help to interpolate the information at 325 MHz, another GMRT frequency band with very little information of suitable phase calibration sources. This database would also be useful at the new low-frequency bands of the upgraded GMRT.

Acknowledgements

We thank the staff of the GMRT that made these observations possible. GMRT is run by the National Centre for Radio Astrophysics of the Tata Institute of Fundamental Research. The VLA is operated by the US NRAO which is operated by Associated Universities, Inc., under cooperative agreement with the NSF.

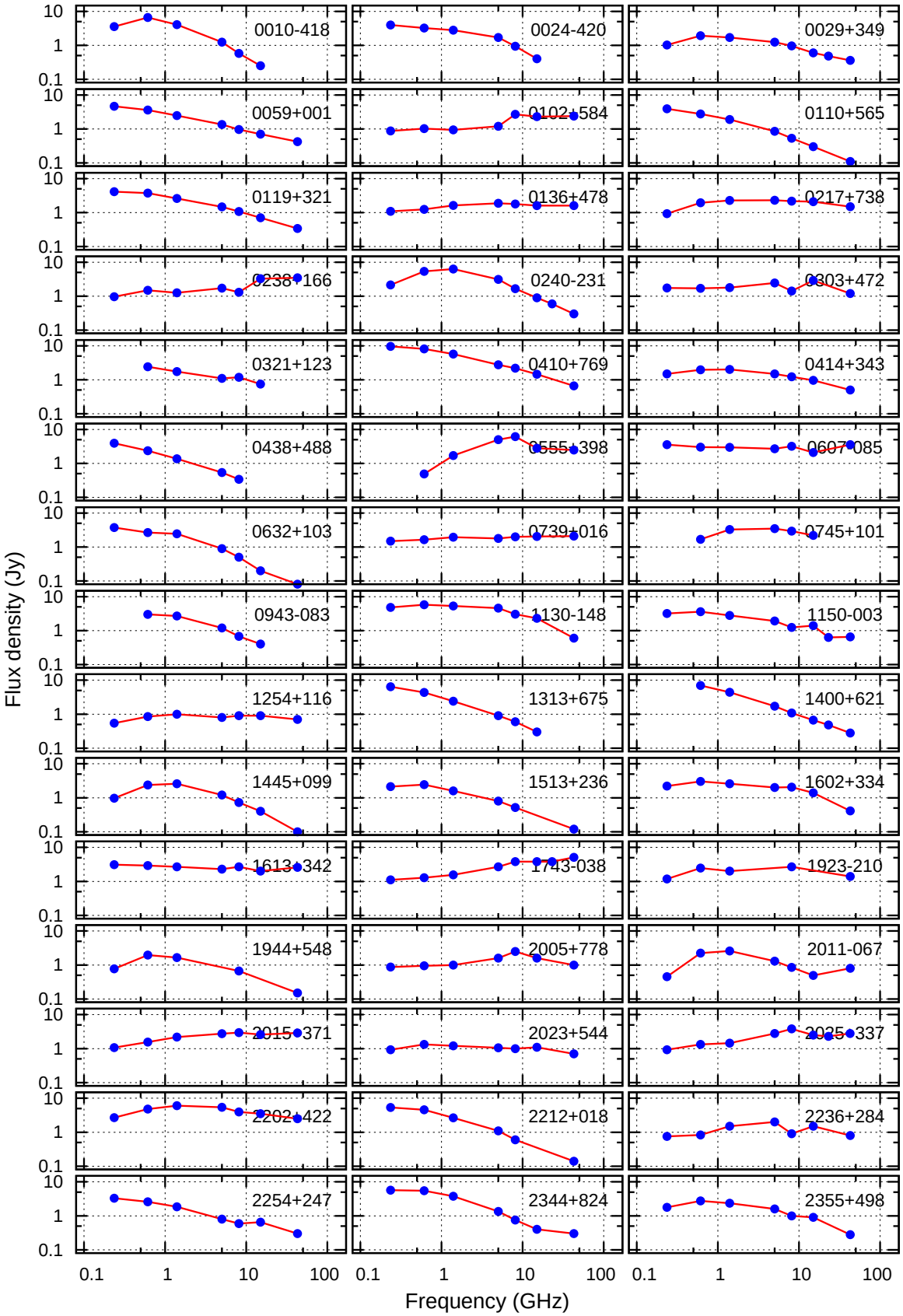

Figure 1: Integrated flux density (spectra) for the calibration sources. Various measurements along with error bars (not plotted) at 235 MHz and 610 MHz are explained in Table 2.

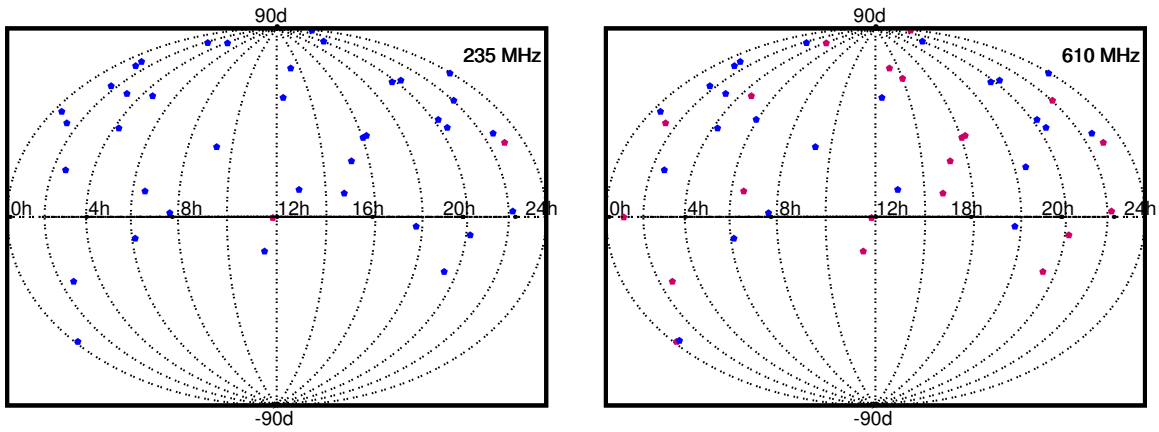

Figure 2: A Mollweide projection plot in equatorial coordinates showing the sky distribution of sources at 235 MHz (left-panel) and at 610 MHz (right-panel). The horizontal and vertical axes in each panel are right ascension and declination, respectively. The legends in the plots, i.e., red and blue points, correspond to the quality factor, good, 'G' and moderate, 'M', respectively (see Sect. 5.1) of the calibration source.

References

Baars, J. W. M., Genzel, R., Pauliny-Toth, I. I. K., & Witzel, A., 1977, A&A, 61, 99
Beasley, A. J. & Conway, J. E., 1995, ASP Conf. Ser., 82, 327
Chengalur, J. N. 2013, NCRA internal technical report, FLAGCAL: A flagging and calibration pipeline for GMRT data
Fomalont, E. B. & Perley, R. A., 1999, ASP Conf. Ser., 180, 79
Intema, H. T., van der Tol, S., Cotton, W. D., et al. 2009, A&A, 501, 1185
Lal, D. V. 2014, NCRA internal technical report, FLAGCAL: Imaging Results
Prasad, J., & Chengalur, J. N. 2012, Exp. Astrn., 33, 157
Swarup, G., Anathakrishnan, S., Kapahi, V. K., et al., 1991, Current Science, 60, 95
Thompson, A. R., Moran, J. M., & Swenson, G. W. 2001, Interferometry and Synthesis in Radio Astronomy, Wiley, USA
The VLA calibrator manual, available at http://www.vla.nrao.edu/astro/calib/manual/
VLA Observational Status Summary, available at https://science.nrao.edu/facilities/vla/docs/manuals/oss

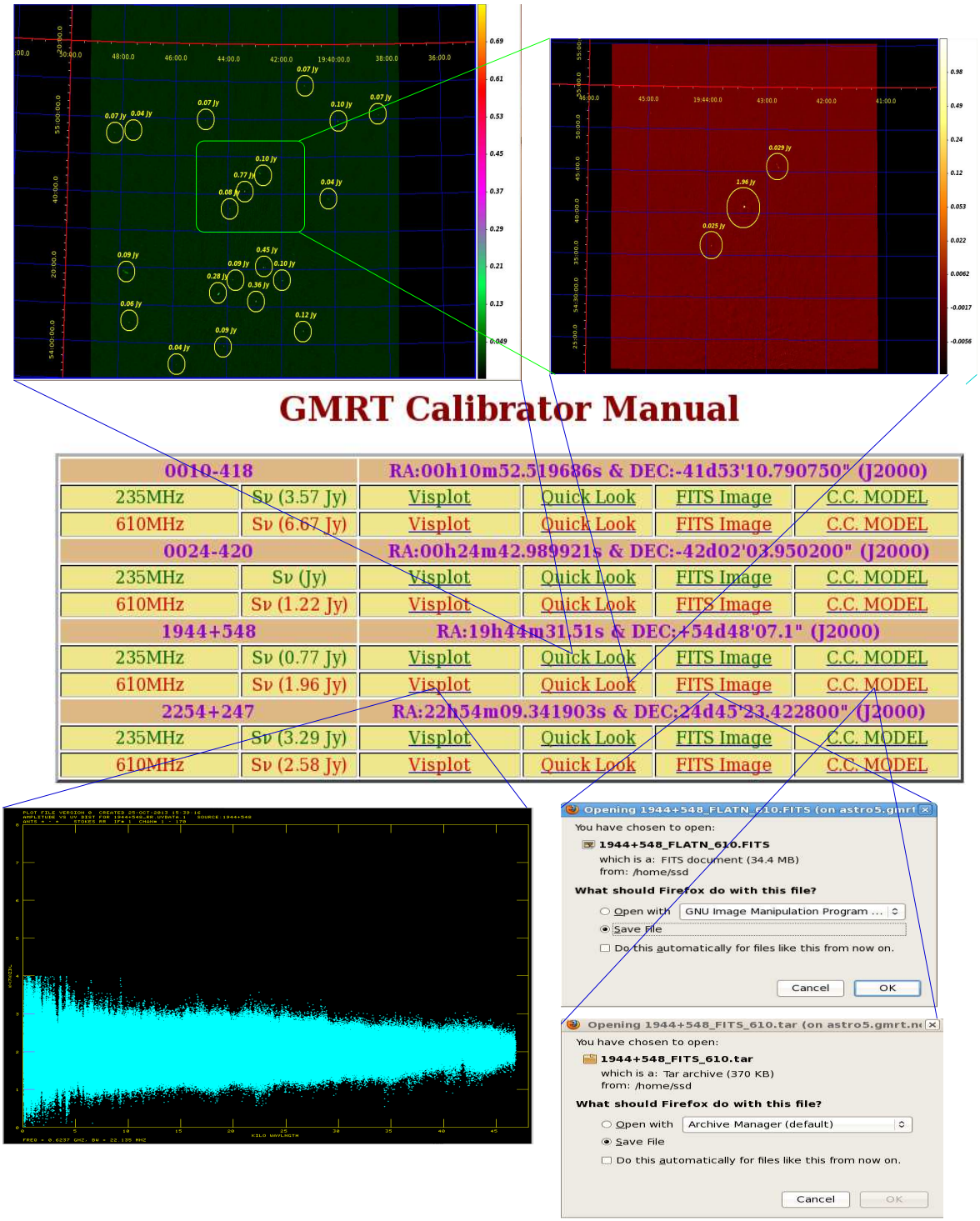

Figure 3: A screen-shot of the GMRT calibrator manual from the online web-page at the GMRT observatory. Top-left panel and top-right are the images of a calibration source at 235 MHz and 610 MHz. All the data products for a calibration source are also listed, including coordinates (α, δ), observing frequency, flux density, (u, v) plot (or visplot), quick-look image of the field-of-view, CLEAN restored model map and CLEAN-component model.